

## 5. SITE 1046<sup>1</sup>

### Shipboard Scientific Party<sup>2</sup>

#### HOLE 1046A

**Position:** 15°32.1912'N, 58°42.8583'W

**Date occupied:** 1945, 31 December 1996

**Spud hole:** 2200, 31 December 1996

**End hole:** 1530, 3 January 1997

**Time on hole:** 2 days, 19 hr, 45 min

**Seafloor depth (drill-pipe measurement from rig floor, m):** 5028

**Distance between rig floor and sea level (m):** 11.0

**Water depth (drill-pipe measurement from sea level, m):** 5017

**Total depth (from rig floor, m):** 5860

**Penetration (m):** 832

**Total core recovered (m):** 0

**Comments:** Logging while drilling (LWD). No coring done. Seafloor depth identified from LWD data.

**Principal results:** Site 1046 was drilled through the décollement zone of the northern Barbados accretionary prism at 1.9 km west of the frontal thrust and about 900 m east of Site 1045. Site 1046 is a reoccupation of Site 949, which was partially cored and instrumented with a CORK borehole seal. The negative polarity reflection that characterizes the décollement zone beneath Site 1045 diminishes in strength laterally to Site 1046. At Site 1046, LWD gamma-ray, resistivity, density, caliper, photoelectric effect, and neutron porosity logs were acquired from the surface through the décollement zone to oceanic basement at 832 m below seafloor (mbsf). Excluding neutron porosity, all logs are of excellent quality.

Traditional visual and multivariate statistical analyses define eight log units (Fig. 1). These log units subdivide into two sedimentary packages corresponding to the sections above and below the décollement zone. Based on correlation with other sites, sediments above the décollement zone are carbonate and clay-rich calcareous claystone and noncalcareous claystone. Log Units 1 through Subunit 3a are dominated by calcareous claystone. Decreasing resistivity in log Subunits 3a and 3b suggests a transition to a more clay-rich lithology above the décollement zone. A low-density interval in log Unit 4 and Subunit 5a correlates with the décollement zone. High gamma-ray and potassium values suggest significant terrigenous input in log Subunits 5b through 6b. The spiky resistivity response in log Unit 6 indicates cyclical sedimentation, probably turbidite deposition. The low resistivity and low gamma-ray values in log Unit 7 suggest pelagic sediment accumulation. Higher gamma-ray and resistivity values in log Unit 8 suggest correlation with the calcareous ferruginous unit cored at the base of Site 543.

Deformational features from the cores and seismic data correlate well with log-inferred structural features. Inversions in the gamma-ray and density curves indicate thrust faults at 162, 225, 260, 288, and 350 mbsf. Results from adjacent Hole 949B, which was cored from 244.1 to 464.2 mbsf, confirm thrusting at 260, at about 280, and at 350 mbsf. Seismic

data indicate a thrust fault at about 286 mbsf that correlates well with the log-inferred thrust at 288 mbsf. The structurally defined décollement zone from the cores lies between 370 and 427 mbsf. A sharp drop in the Site 1046 LWD density curve suggests that the top of the décollement zone is at 380 mbsf. The lower contact of the décollement zone is indistinct, but appears consistent with the core data. Broad geochemical anomalies and a lack of thermal anomalies around the faults and décollement zone at Site 949 suggest that fluid flow is not currently active along these structures. The synthetic seismogram reproduces the reflection at the thrust fault at about 280 mbsf, but identifies the décollement zone only weakly.

The density log agrees well with all available core densities at Site 949, except those from the carbonate-rich zone at 300–322 mbsf (Fig. 2). Comparisons of mean densities through the décollement zone at Site 1046 and an equivalent sequence at reference Site 1044 suggest selective consolidation of this interval, assuming equivalent starting densities. In addition, the décollement zone at Site 1046 is significantly more consolidated than the equivalent sequence at Site 1045.

#### BACKGROUND AND OBJECTIVES

Site 1046 is 1800 m west of the frontal thrust of the accretionary prism (Fig. 3A). Here, the seismic reflection data indicate that the accretionary prism is thickened by at least one prominent thrust fault at about 286 mbsf and is underlain by a probable décollement-zone reflector at about 400 mbsf (Fig. 4). Seismic reflection data show that the oceanic crust reflector is at about 850 mbsf. From Site 1045 seaward to Site 1046, the amplitude of the décollement reflector decreases substantially (Figs. 3B, 4). Site 1046 is located close to Hole 949C, where a CORK is installed (Fig. 5). Although incompletely cored, adjacent Hole 949B shows structural and stratigraphic evidence for thrust faulting and a weakly developed décollement zone (Shipboard Scientific Party, 1995b).

An objective of Site 1046 was to measure the physical properties of a décollement zone with intermediate reflection polarity characteristics. We anticipate comparison of the physical properties of the décollement zone at Site 1046 with those at Site 1045, where the décollement zone has a high-amplitude negative polarity. Penetration of several thrust faults above the décollement zone will further define the log character of faults in the accretionary prism. The logs at Site 1046 will specify the physical properties profile at this CORK locality and will support interpretation of the hydrogeologic testing results (e.g., Sreaton et al., 1997). Another objective was to relate the seismic compressional (*P*-wave) and shear (*S*-wave) velocities determined from vertical seismic profiles (VSPs) in Hole 949C (Shipboard Scientific Party, 1995b) to physical properties of the sediments in order to extrapolate these properties away from the hole.

Drilling at Site 1045 did not significantly penetrate the underthrust section, because of unstable hole conditions beneath the décollement zone. Therefore, another primary objective at Site 1046 was to penetrate the underthrust section to the oceanic basement. We planned to evaluate the consolidation of the underthrust section caused by burial by the overlying accretionary prism. Water produced by the consolidation of the underthrust section drives the hydrologic system (Sreaton et al., 1990; Bekins et al., 1995) and controls faulting. Comparison of lithologic and porosity data from Sites

<sup>1</sup>Moore, J.C., Klaus, A., et al., 1998. *Proc. ODP, Init. Repts.*, 171A: College Station, TX (Ocean Drilling Program).

<sup>2</sup>Shipboard Scientific Party is given in the list preceding the Table of Contents.

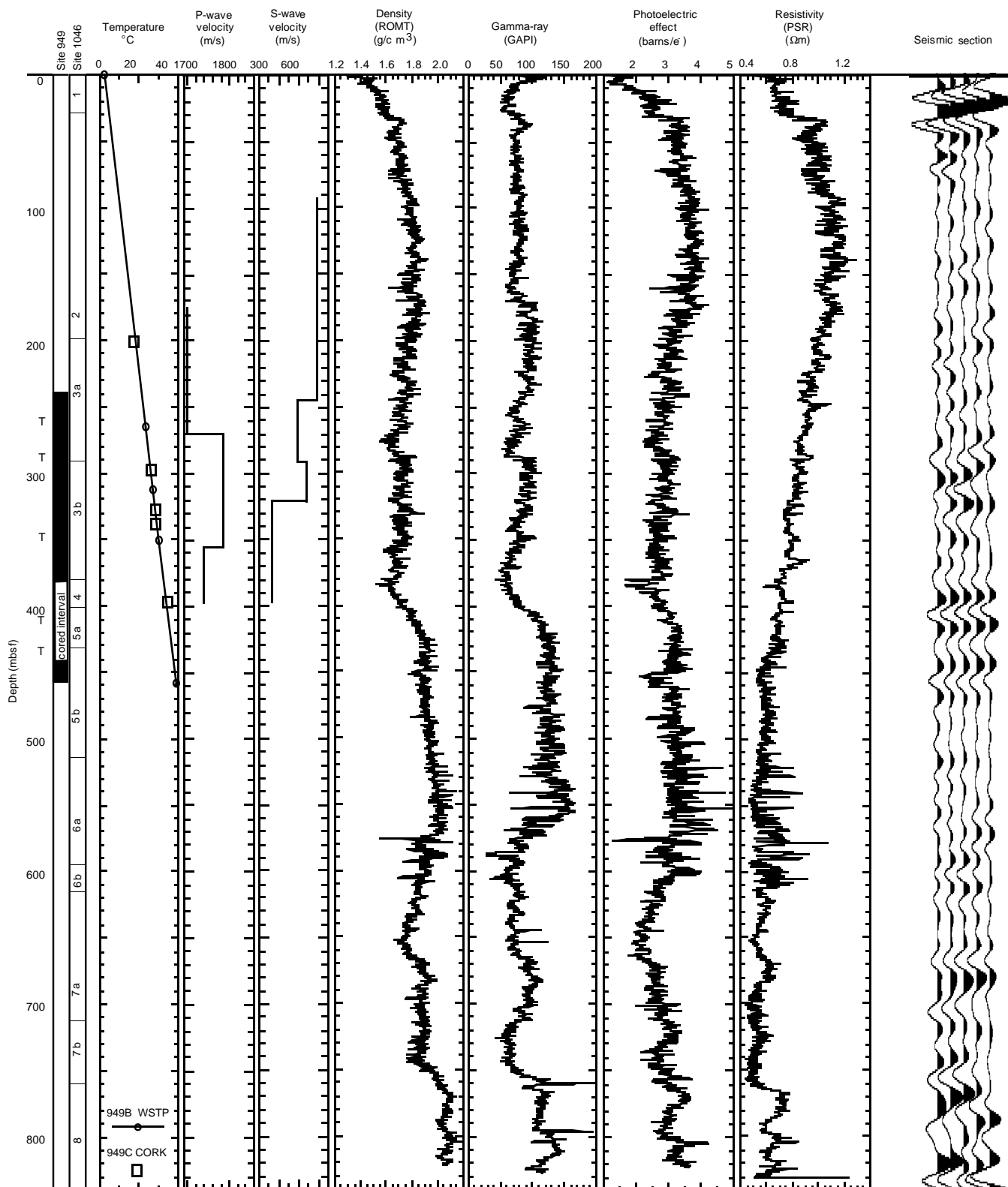


Figure 1. Comparison of LWD data from Hole 1046A with seismic velocities from VSPs in Hole 949C and downhole water sampler, temperature, and pressure probe (WSTP) temperature measurements from Hole 949B and the Hole 949C CORK. Also shown is a short strip of the seismic section through Hole 1046A (Line 735 common midpoint 1227). Log units and fault zones recognized in the core (marked "T") are shown on the left.

1044 and 1046 will determine the magnitude of water flux from the underthrust sediments during initial subduction.

## OPERATIONS

### Hole 1046A

After pulling out of Hole 1045A, the drill string was raised to 50 m above the seafloor, and the vessel was offset in dynamic positioning mode to Site 1046 (proposed site NBR-9A). Hole 1046A was spudded at 2200 hr, 31 December 1996, at 15°32.1912'N, 58°42.8583'W. This location is ~50 m south of the Hole 949C reentry cone and CORK installation. Drilling was initiated at a water depth of 5021.4 m below rig floor (mbrf), based on the precision depth recorder (PDR) reading. The final water depth was established at 5028 mbrf (5017 m below sea level [mbsl]), based on analysis of the LWD data.

The décollement zone for Site 1046 was estimated to be at 424 mbsf. We attempted to drill at 35 m/hr down to 5487 mbrf (459 mbsf), where high torque and pump pressures were encountered. The drill string was pulled back to 362 mbsf, with a maximum drag of 50,000 lb. The hole was washed and reamed for 3 hr in the décollement zone from 362 to 459 mbsf. All drilling parameters returned to normal and drilling resumed at 459 mbsf. No further difficulties were experienced, and the hole was drilled at about 35 m/hr to a total depth of 5860 mbrf (832 mbsf), where basement was found and the drilling rate was slowed to 6 m/hr. Hole 1046A was terminated at 5860 mbrf (832 mbsf), with the depth objective successfully achieved. Average LWD drilling parameters during Hole 1046A were 0–15,000 lb weight on bit (WOB), 40–55 rpm, 300–550 psi, 100–200 A torque, and 35 m/hr rate of penetration (ROP).

The drill string was raised to 400 mbsf, and the hole was displaced with 130 barrels of heavy (11.0 lb/gal) mud. The trip continued to the surface, where the nuclear sources were removed, the LWD data were retrieved, and the LWD collars were laid out. The bit cleared the rotary table at 1530 hr on 3 January 1997, ending drilling in Hole 1046A.

## CHARACTERIZATION OF LOGS

### Definition of Log Units

The log data, with the log units labeled, are shown in Figure 6. Eight log units and several subunits were defined through a combination of visual interpretation and multivariate statistical analysis (Fig. 7; see “Explanatory Notes” chapter, this volume).

Three factors were extracted from the deep resistivity, gamma-ray, thorium, potassium, photoelectric effect, and bulk density logs. Because of a large scatter in the data and lack of log character, the neutron porosity data were not used. The three factors explain 90% of the variance contained in the data. The cluster analysis shows five prominent clusters. Table 1 summarizes the mean values and standard deviations of the log properties by cluster, each of which shows a distinct set of physical properties. Figure 7 shows the calculated cluster log, together with the log units, gamma ray, and density.

The base of Unit 1 (0–34.5 mbsf) is defined by positive shifts in the resistivity and photoelectric effect of 0.3  $\Omega\text{m}$  and 1.0 barns/e<sup>-</sup>, respectively.

Log Unit 2 extends from 34.5 to 190.0 mbsf. Only subtle gradational changes in log character occur across the log Unit 2/3 boundary (Fig. 7; Table 1). The neutron porosity standard deviation increases from 0.036 to 0.062 across the log Unit 2/3 boundary.

Log Unit 3 (190.0–379.8 mbsf) is generally characterized by gradational decreases in resistivity and bulk density. The base of Subunit 3a (190.0–287.9 mbsf) is the bottom of a decreasing gamma-ray trend and is the top of a second decreasing gamma-ray trend. The base of Subunit 3b is at a local minimum of 55 GAPI in the gamma

ray. The photoelectric effect at the base of Subunit 3b (287.9–379.8 mbsf) has a negative shift of 0.8 barns/e<sup>-</sup>.

Log Unit 4 (379.8–390.3 mbsf) corresponds to the upper negative polarity reflector that may be associated with the décollement zone and shows a negative shift in the photoelectric effect to 2.5 barns/e<sup>-</sup>. In this zone, there is also a slight negative shift in density of 0.1 g/cm<sup>3</sup>. Log Unit 4 is not well defined in the resistivity logs.

Log Unit 5 (390.3–511.7 mbsf) is divided into two subunits. The base of Subunit 5a (390.3–439.4 mbsf) is at a positive shift in the potassium and an increase in the potassium variability. The base of Subunit 5b (390.3–439.4 mbsf) is inferred to be the top of the turbidite section. There is an increase in the standard deviations of the resistivity, gamma ray, density, and photoelectric effect of 0.009  $\Omega\text{m}$ , 1.1 GAPI, 0.003 g/cm<sup>3</sup>, and 0.15 barns/e<sup>-</sup>, respectively, at the log Unit 5/6 boundary (Fig. 7; Table 1).

Log Unit 6 extends from 511.7 to 613.1 mbsf. The gamma ray in Subunit 6a (511.7–586.4 mbsf) decreases below 555 mbsf. The minimum in the decreasing gamma-ray trend is the base of Subunit 6a. There are also negative shifts in the density and photoelectric effect logs at the Subunit 6a/6b boundary. The standard deviation of the resistivity, gamma ray, and photoelectric effect decreases by 0.02  $\Omega\text{m}$ , 14 GAPI, and 0.16 barns/e<sup>-</sup>, respectively, at the base of Subunit 6b (586.4–613.1 mbsf).

Log Unit 7 (613.1–756.2 mbsf) is generally characterized by low resistivity (mean of 0.565  $\Omega\text{m}$ ) and low neutron porosity (mean of 0.55). The base of Subunit 7a (613.1–711.1 mbsf) is defined by negative shifts in the gamma ray and photoelectric effect of 20 GAPI and 0.14 barns/e<sup>-</sup>, respectively. The base of Subunit 7b is at a negative photoelectric effect and bulk density shift, but is best seen in the cluster analysis (Fig. 7). Log Unit 8 (756.2–820.5 mbsf) is characterized as a zone of high gamma ray (mean of 124.6 GAPI) and high bulk density (mean of 1.97 g/cm<sup>3</sup>).

### LWD Log Quality

For Hole 1046A, a target ROP (1.5 m averaged) of 35 m/hr was used, because we concluded that gamma-ray spectrometry data collected by the natural gamma-ray tool (NGT) at 30–40-m/hr penetration rates are reliable in Hole 1044A (see “Characterization of Logs” section, “Site 1044” chapter, this volume). An ROP of ~35 m/hr was maintained throughout Hole 1046A (Fig. 8).

The differential caliper values in Hole 1046A show standoffs of <1 in, except for an interval at 0–4 mbsf and at 576 mbsf (1.04 in). Zones of minor washout are identified in the intervals 0–40, 160–165, 178–185, 332–345, 365–372, 380–387, 450–460, 573–590, and 810–817 mbsf. Overall, borehole conditions were excellent; 99.4% of the hole showed a differential caliper of <1 in, and 96.4% showed values <0.5 in. The bulk density correction (DRHO) varies from -0.09 to 0.05 g/cm<sup>3</sup>, indicating the high quality of the density measurements. Time-after-bit (TAB) measurements are 10 to 40 min for resistivity and gamma-ray measurements and 30 to 80 min for density and neutron porosity measurements. High TAB values (as much as 200 min) in the interval from 448 to 462 mbsf coincide with a wiper trip. The wiper trip interval, in turn, coincides with the minor washout interval at 450–460 mbsf; however, the differential caliper and DRHO logs indicate that the borehole conditions did not deteriorate significantly during the wiper trip (i.e., between the time of drilling and time of measurement).

## LOGS AND LITHOLOGY

Site 1046 is located within about 60 m of the three holes drilled at Site 949. Although only 220 m of the section at Site 949 was cored and core recovery was quite poor, the lithology above the décollement zone can be correlated with the logs collected at Site 1046. The

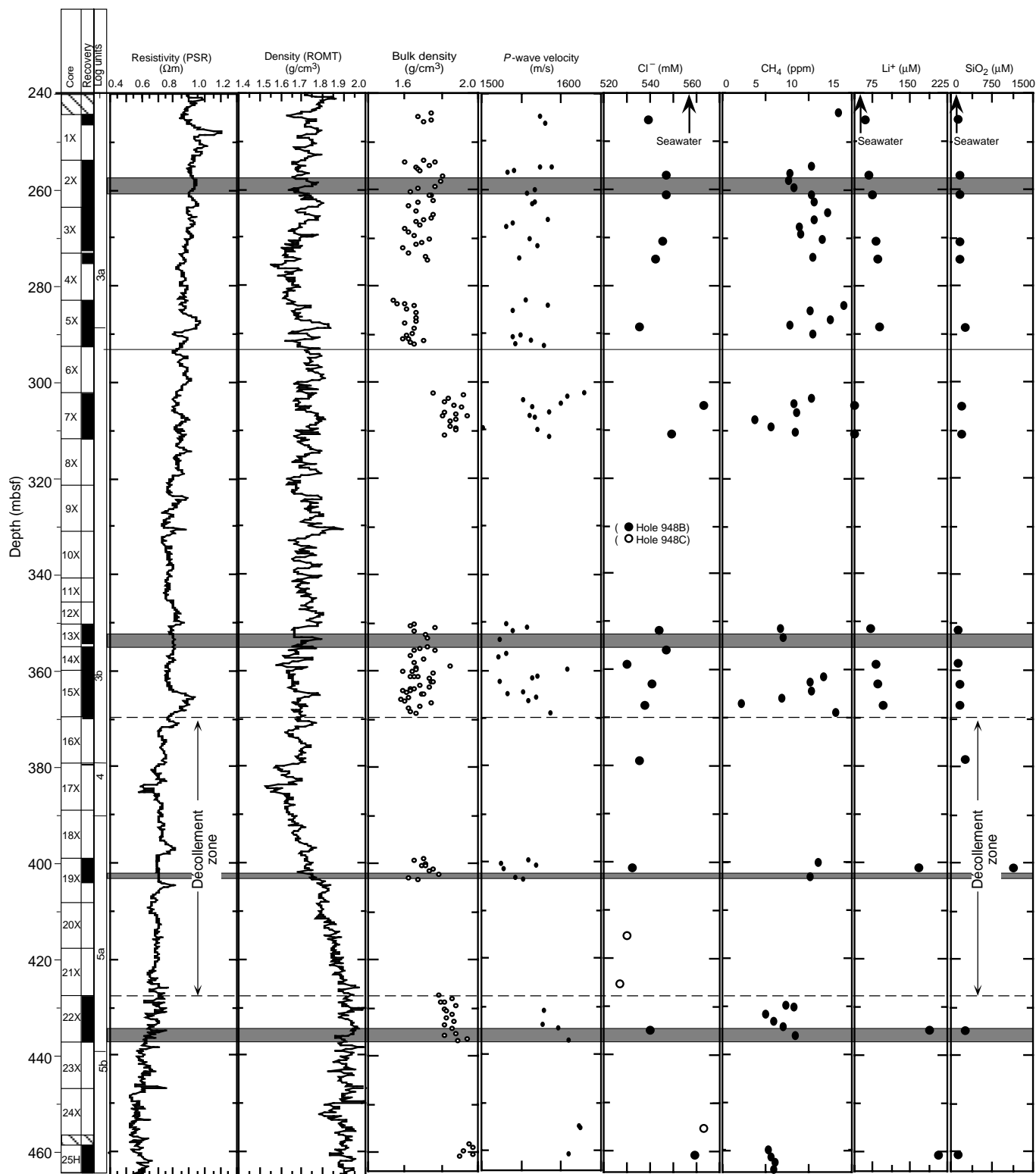


Figure 2. Summary of log data from Hole 1046A and core data from Holes 949B and 949C. Log units for Hole 1046A are shown beside the lithologic units for Hole 949B. Shaded bars are fault zones identified in the core. Dashed lines indicate maximum limits of the décollement zone, as indicated by cores at Site 949. The XRD clay mineralogy column is a three-part subdivision of the %total clay of the XRD mineralogy column.

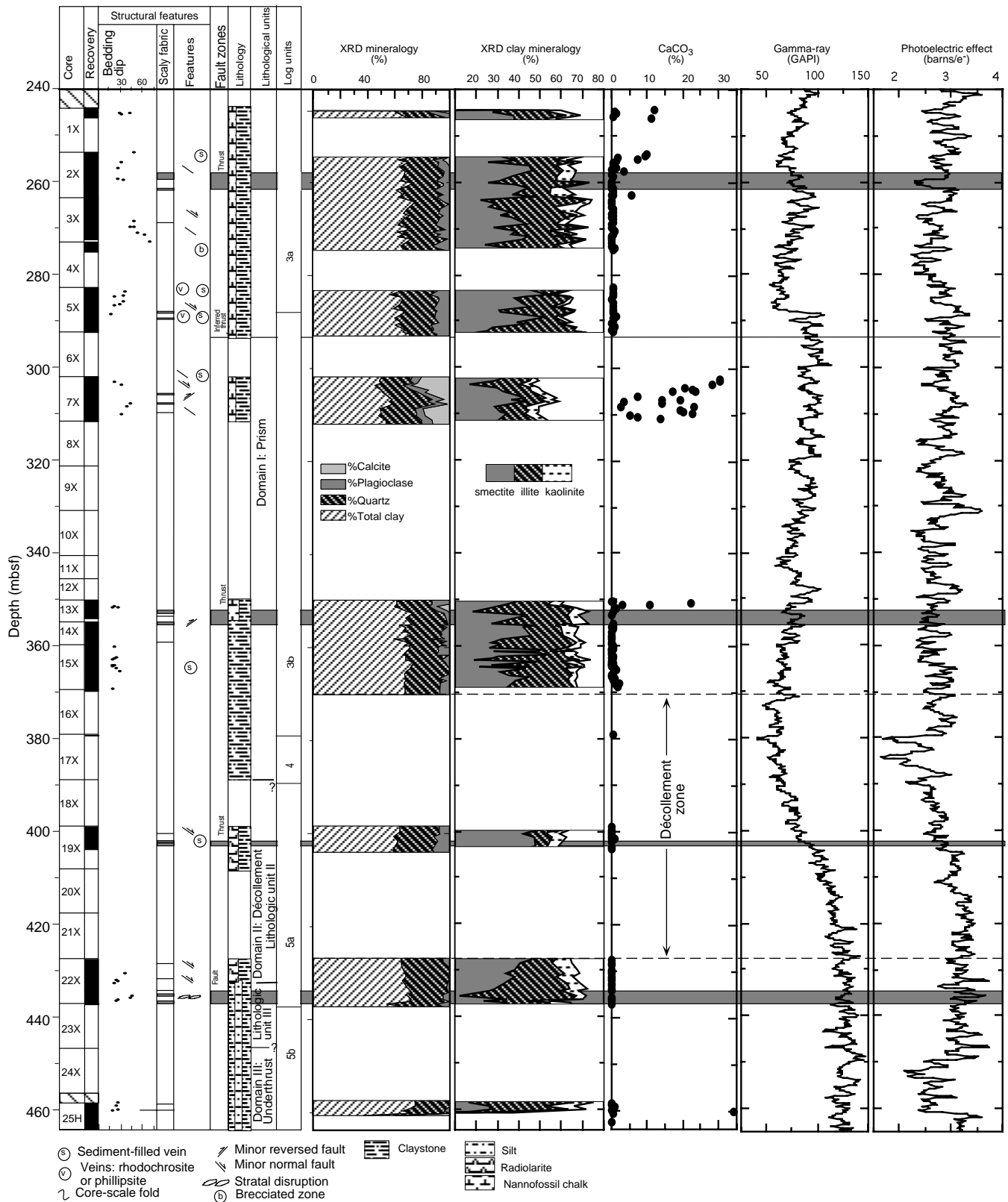


Figure 2 (continued).

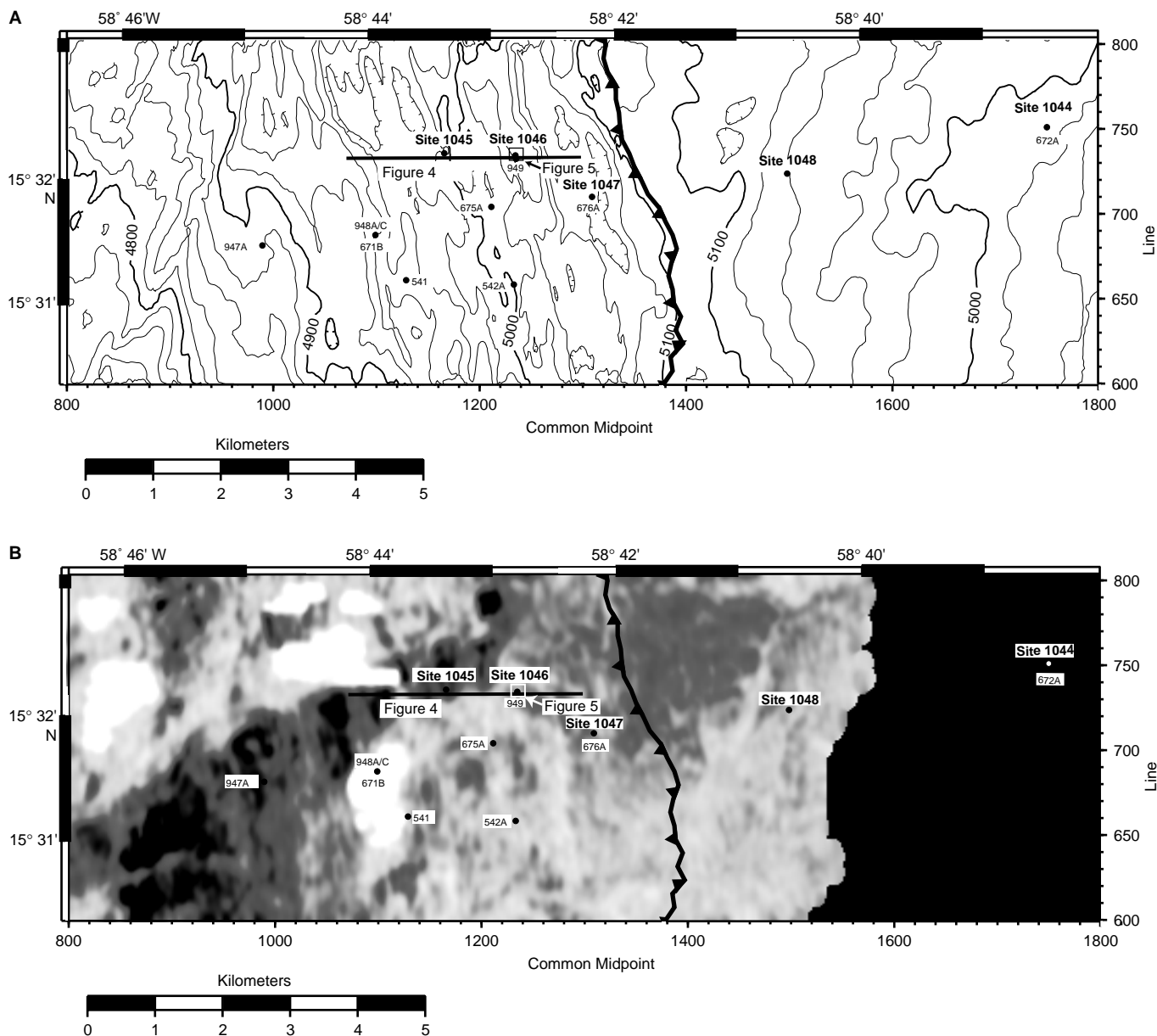


Figure 3. **A.** Bathymetric location map for Site 1046 in the Leg 171A drilling area and for previous Ocean Drilling Program and Deep Sea Drilling Project holes in the northern Barbados accretionary prism. **B.** Map of peak seismic amplitude of the décollement-zone reflector of the northern Barbados accretionary prism in the Leg 171A drilling area.

Site 949 lithologic units were similar to those recovered at Site 948, which is 2.5 km away. Lithologic units below the décollement zone may be correlated with those from the reference Site 672, as the log character in the underthrust section is similar to that at Site 1044.

The lithologic descriptions from Site 949 are summarized below. A stratigraphic column is shown in Figure 6 in the “Logs and Lithology” section of the “Site 1045” chapter (this volume).

**Site 949**

**Lithologic Unit I (0–2.95 mbsf)**

Unit I was sampled only in the mudline core. The unit comprises moderately bioturbated calcareous clays containing variable abundances of nannofossils and foraminifers. Thin interbeds of ash are

common. Sediments recovered in the upper section of Site 676 (1.4 km southeast of Site 949) are similar to those of this unit, suggesting a thickness of 160 m for Unit I.

**Lithologic Unit II (244.1–430.92 mbsf)**

The thickness of Unit II is due in part to repeated sections that result from thrust faults splaying off the décollement zone. Unit II is divided into three subunits, which can be correlated with three of the five subunits of Unit II at Site 948 a few kilometers away. These are Site 948 Subunits IIB, IIC, and IIE. Subunit IIB contains nannofossil-bearing clay and rare volcanic ash. Carbonate content within this subunit is variable, but consistently higher than in the adjacent units. Subunit IIB is repeated at least twice within the cored section. The

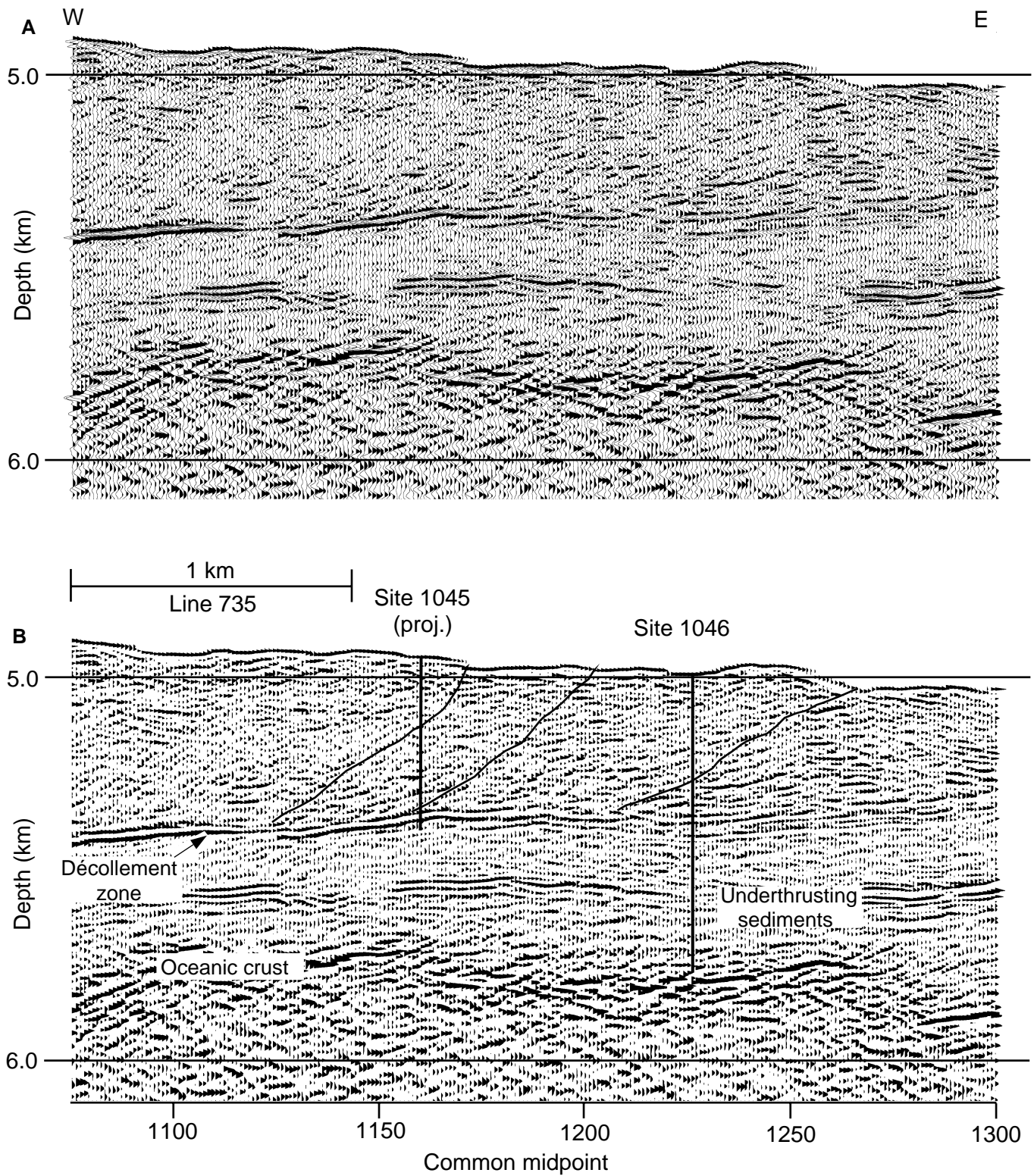


Figure 4. (A) Uninterpreted and (B) interpreted seismic Line 735 through Site 1046 (see Fig. 3 for location). Black = positive polarity; white = negative polarity. The amplitude of the negative polarity reflection decreases from beneath Site 1045 to Site 1046.

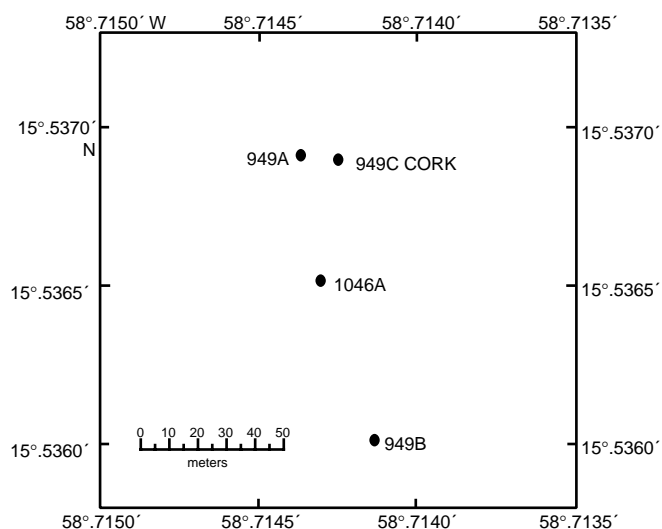


Figure 5. Location of Site 1046, cored Holes 949A and 949B, and CORK Hole 949C. See inset box of Figure 3A for location.

upper interval extends from 244.1 to 255.4 mbsf, and the lower interval extends from 302.1 to 353.88 mbsf. Subunit IIC is composed of mottled claystones with a low carbonate content, repeated by thrusting 255.4 and 298 mbsf and 353.88 and 388.80 mbsf. Subunit IIE is recognized by a high radiolarian content. A thrust repetition within Subunit IIE occurs at 402.82 mbsf, placing lower lower Miocene strata over upper lower Miocene deposits.

#### **Lithologic Unit III (430.92–464.2 mbsf)**

Only about 33 m of Unit III was recovered at Site 949. It is characterized by mottled, variegated claystones, with interbeds of sandy siltstone, siltstone, clayey siltstone, and nanfossil-bearing siltstone. Interbeds generally have a sharp base, commonly with laminations or cross-bedding near the base, and fining-upward sequences in the top portion. Carbonate content is generally low and sharply partitioned between beds.

#### **Bulk Mineralogy**

Unlike at Site 948, no significant changes in mineralogic character occur across the lower boundary (430.92 mbsf) of Unit II at Site 949. Calcite percentages from X-ray-diffraction (XRD) analysis are effectively zero, except within the nanfossil-rich claystone of Subunit IIB (244.1–255.4 and 302.1–353.88 mbsf) and carbonate turbidites of Unit III (430.92–464.2 mbsf), where the maxima are 28% and 37%, respectively. Quartz content is fairly constant between 22% and 30% throughout Hole 949B. Plagioclase content ranges from trace amounts to 14%. Generally, less plagioclase occurs in claystones below 425 mbsf. Total clay mineral contents range from 56% to 74% within carbonate-free claystones and drop to values of 36% to 56% within the nanfossil-rich claystones. The total clay mineral content appears to increase slightly near the décollement zone.

#### **Correlation With Log Units**

LWD results at Site 1046 indicate the presence of two distinct, major sedimentary packages corresponding to the sections above and below the décollement zone. Figure 9 shows a correlation linking the upper overthrust prism section to the section logged at Site 1045 and the lower underthrust section to the section logged at reference Site 1044.

Sediments above the décollement zone are constrained to ash-rich calcareous claystones and noncalcareous claystones. These two major sediment types are present in the reference section above the proto-décollement zone and are stacked by imbricate thrust faults within the accretionary prism. Log Unit 1 is characterized by increasing photoelectric effect with depth, which is probably partially because of the increase in density caused by sediment compaction. High photoelectric effect is also probably related to a relatively high carbonate content in the upper part of the hole. The mudline core from Site 949 contained sediments relatively high in carbonate content, which is consistent with both the high photoelectric effect in the Site 1046 logs and the calcareous sediments recovered in the upper part of Sites 672 and 671. The interval from log Unit 1 through Subunit 3a shows overall trends in gamma ray, density, and photoelectric effect that are similar to trends in log Unit 1 at Site 1044 and Units 1 through 5 at Site 1045; this suggests an increase in clay content and/or a decrease in carbonate with depth through this interval. The values of these three logs at Site 1044 are slightly lower than those at Site 1046, which may be attributed to greater compaction of the sediments within the prism. This section at Site 1044 has been described as representing carbonate- and ash-rich claystones overlying carbonate- and ash-poor claystones, whereas the greater thickness of the section at Site 1046 is thought to be caused by thrust faulting (see “Logs and Structure” section, this chapter).

Log Subunit 3b shows similar trends and absolute values in the gamma-ray, photoelectric effect, and density logs. The decrease in the gamma ray from more than 100 to about 65 GAPI, which repeats in both Subunits 3a and 3b (190–287.9 and 287.9–379.8 mbsf, respectively), is probably caused by the decreasing ash content of the sediments. The presence of pore-water anomalies and a large-scale thrust fault in the seismic section at the level of the Subunit 3a/3b boundary suggests the presence of a major thrust fault that results in more than 90 m of repeated section, or the entire thickness of log Subunit 3b. The inference of thrust repetition made from the logs is consistent with paleontologic and lithostratigraphic data from Site 949, which also show evidence of a thrust at 295 mbsf.

Log Unit 4 represents the top of the décollement zone identified at Site 949. Although core recovery in this interval at Site 949 was poor, the cores constrain the placement of the radiolarian-rich unit associated with the décollement zone at other sites to between 388.8 and 430.92 mbsf. This corresponds approximately to log Unit 4 and log Subunit 5a, both of which show a steady increase in gamma ray, density, and photoelectric effect. An increase in the thorium/potassium ratio to values >10 in the lower part of log Subunit 5a suggests the presence of smectite, which is seen below the décollement zone at Sites 672 and 671 (Tribble, 1990), although clay analyses of samples from Site 949 indicate the dominance of illite at this level (Underwood and Deng, 1997). The high thorium/potassium ratios could also be the result of anomalously low potassium levels, rather than increased thorium, which may indicate that a factor other than clay mineralogy, such as ash content, is controlling the ratio.

The section below the décollement zone, comprising log Units 5 through 8, bears a close resemblance to the comparable section at Site 1044. Log Subunit 5b correlates with lithologic Unit III at Site 672 and the lower part of log Unit 3 at Site 1044. The correlation between the lower sections of Sites 1046 and 1044 and the resulting similarities are displayed in Figure 9. Log Subunit 5b corresponds to an interval of interbedded marlstones and claystones, inferred from high variability in the photoelectric effect and gamma-ray logs. Log Subunits 6a and 6b, which show even greater amplitude variation in the photoelectric effect and gamma-ray logs, correlate with the turbidite section recognized at Site 1044 (log Subunits 4a and 4b). The upward decrease in gamma ray through the cyclically bedded sediments (Subunits 5b, 6a, and 6b) could reflect the decreasing importance of terrigenous input to this site during the mid-Tertiary. The thickness of the cyclically bedded sediments, including the interbedded marl-

stones and claystones and the turbidites, appears to be significantly less at Site 1046 than at the reference site. Several factors could account for the thinning: differences in depositional environment, loss of section from normal faulting, and compaction within the turbidites.

Log Subunits 7a and 7b correlate with log Unit 5 at Site 1044. Although lithologic control was rather poor in this section, correlation with the sediments recovered at Site 543 indicates the presence of Eocene zeolite-bearing claystones at this stratigraphic level. The increases in density, gamma ray, and resistivity at the bottom of Subunit 7a are thought to be caused by a particularly zeolite-rich interval. This section also shows <10% thinning from the reference site to Site 1046. Finally, log Unit 8 at Site 1046 correlates with the dolomitized ferruginous claystones that overlie basement at Site 543.

## LOGS AND STRUCTURE

Site 1046 is located ~60 m from Hole 949B, cored from 244.1 to 464.2 mbsf during Leg 156. Structural features interpreted from the seismic reflection data are correlatable within 10 m depth between holes, making the comparison of core data to LWD data reasonable. This section compares structural features in core, seismic, and LWD data, which are summarized in Figure 10.

Core recovery was poor in Hole 949B. Core deformation structures consisted of scaly fabric, sediment- and mineral-filled veins, breccia zones, stratal disruption, and discrete normal and reverse faults (Shipboard Scientific Party, 1995a). Significant thrusts were identified at 260, 350, and 403 mbsf, based on thick sections of well-developed scaly fabric and biostratigraphic inversions. The upper two thrusts correlate well with significant perturbations in the LWD logs—primarily in gamma ray, but also in density—with less significant impact on resistivity (Fig. 10). The lowest thrust (403 mbsf) lies within the interval ascribed to the décollement zone and most likely represents a small portion of a much thicker fault zone. Although core recovered between 427 and 437 mbsf was previously interpreted to lie within the décollement zone at Site 949 (Shipboard Scientific Party, 1995b), the core contains only one 1-cm-thick zone of horizontal scaly fabric and numerous high-angle normal faults that we attribute to vertical loading of underthrust material below the décollement zone. This normal fault zone correlates with a marked change in trend in the LWD logs at the boundary between log Subunits 5a and 5b. The position of the décollement zone is therefore constrained by core data to above 427 mbsf and below an undisturbed section of core from 360 to 370 mbsf.

Based on core data, an additional thrust fault was previously inferred at 295 mbsf. However, no fault material was recovered. Consequently, the location of the thrust was chosen based on a biostratigraphic inversion located somewhere between 260 and 305 mbsf, and on a geochemical anomaly identified in the core between 283 and 293 mbsf at Site 949 (Shipboard Scientific Party, 1995b). Structural features in this cored interval are dominated by subvertical sediment- and mineral-filled veins and high-angle normal faults. We interpret these structures to represent subvertical maximum principal stress and elevated fluid pressures leading to subvertical hydrofracture. Similar features are present in core from 395 to 405 mbsf, directly beneath a thrust fault. Based on this relationship, we suggest relocation of the inferred thrust to above the cored interval, at ~280 mbsf, which correlates with the dominant thrust indicated on seismic reflection data (Fig. 4), and with a large perturbation in the LWD logs at the boundary between log Subunits 3a and 3b (Figs. 10, 6).

Three features are identified on the seismic reflection data: a thrust at 286 mbsf and two negative polarity reflectors at 380 and 432 mbsf, the latter of which is in the vicinity of the décollement zone. The thrust at 286 mbsf separates gently dipping strata in the footwall from more steeply dipping strata in the hanging wall, consistent with

bedding dip data collected from cores (Fig. 10). This fault correlates well with large perturbations in the LWD logs that mark the boundary between log Subunits 3a and 3b. The top of the upper negative polarity reflector is within the possible décollement zone interval defined by core data and correlates with a reversal in trend of both the gamma-ray and density logs (Fig. 10) that occurs within log Unit 4 (Fig. 6). The top of the lower negative polarity reflector correlates with the boundary between log Subunits 5a and 5b (Fig. 6) and the normally faulted core interval and is inferred to lie below the décollement zone. Interpretation of the seismic data suggests that the décollement zone lies between the two negative polarity reflections, further constraining its location to between 380 and 435 mbsf (see “Logs and Seismic Data” section, this chapter). The negative polarity reflectors may be stratigraphic features inherited from the incoming sedimentary section.

Two additional faults are indicated across the LWD logs at 162 and 225 mbsf (Fig. 10). These faults are inferred from shifts in the density and gamma-ray logs that have a similar character to those correlated either with seismically or core-defined faults at 260, 286, and 350 mbsf. The LWD log perturbations associated with these inferred faults are smaller in magnitude than those from the major thrust at 286 mbsf, and these faults are thought to have smaller displacement.

## LOGS AND PHYSICAL PROPERTIES

One of the primary objectives of drilling at Site 1046 was to evaluate physical properties characteristics of the décollement zone and other structural discontinuities apparent in the seismic section. As Site 1046 is ~60 m from Hole 949B, which was drilled and partially cored during Leg 156, the physical properties data from Site 949 core can be correlated with the Site 1046 logging results.

### Density

Variations in the downhole profile of the density log in most of the accreted section at Site 1046 seem strongly controlled by structural features, as is evident in both seismic data and previous drilling (Shipboard Scientific Party, 1995b). In the underthrust section, the density and shallow and deep resistivity logs seem to be dominated largely by trends inherited from the reference section (Table 2; Fig. 11A).

The top part of the section in Hole 1046A displays a downhole density trend that indicates a normal consolidation process, with an average density of 1.56 g/cm<sup>3</sup>. It is offset by a peak in density at 42 mbsf, which is probably related to a structural discontinuity. Below 42 mbsf, the same clearly defined consolidation trend continues to 162 mbsf, where it is sharply offset to higher density values. Between 162 and 285 mbsf, density values decrease linearly, with an upward offset at 225 mbsf. Between 285 and 350 mbsf, the density values show no obvious trend with depth, with an average value of 1.73 g/cm<sup>3</sup>. Core recovered at Site 949 (Shipboard Scientific Party, 1995b) shows a thrust at about 296 mbsf (see “Logs and Lithology” section, this chapter), below which lithologic Subunits IIB and IIC are duplicated. The density log between 285 and 350 mbsf is not obviously a repeat of the log between 162 and 285 mbsf (unlike the gamma-ray log [Fig. 10], which clearly shows the duplication).

The top of the décollement zone at 382 mbsf is indicated by a clear offset in the density profile at this depth, with density values sharply increasing from about 1.6 to 1.95 g/cm<sup>3</sup> over the 50-m interval to 432 mbsf. At 432 mbsf, the increase in density with depth becomes more gradual. Below an inflection point at 570 mbsf, that trend reverses to a downhole decrease in density, similar to a pattern seen in the reference section at Site 1044. Similarly, the changes in the downhole density trend at 650, 680, 745, and 770 mbsf (Table 2;

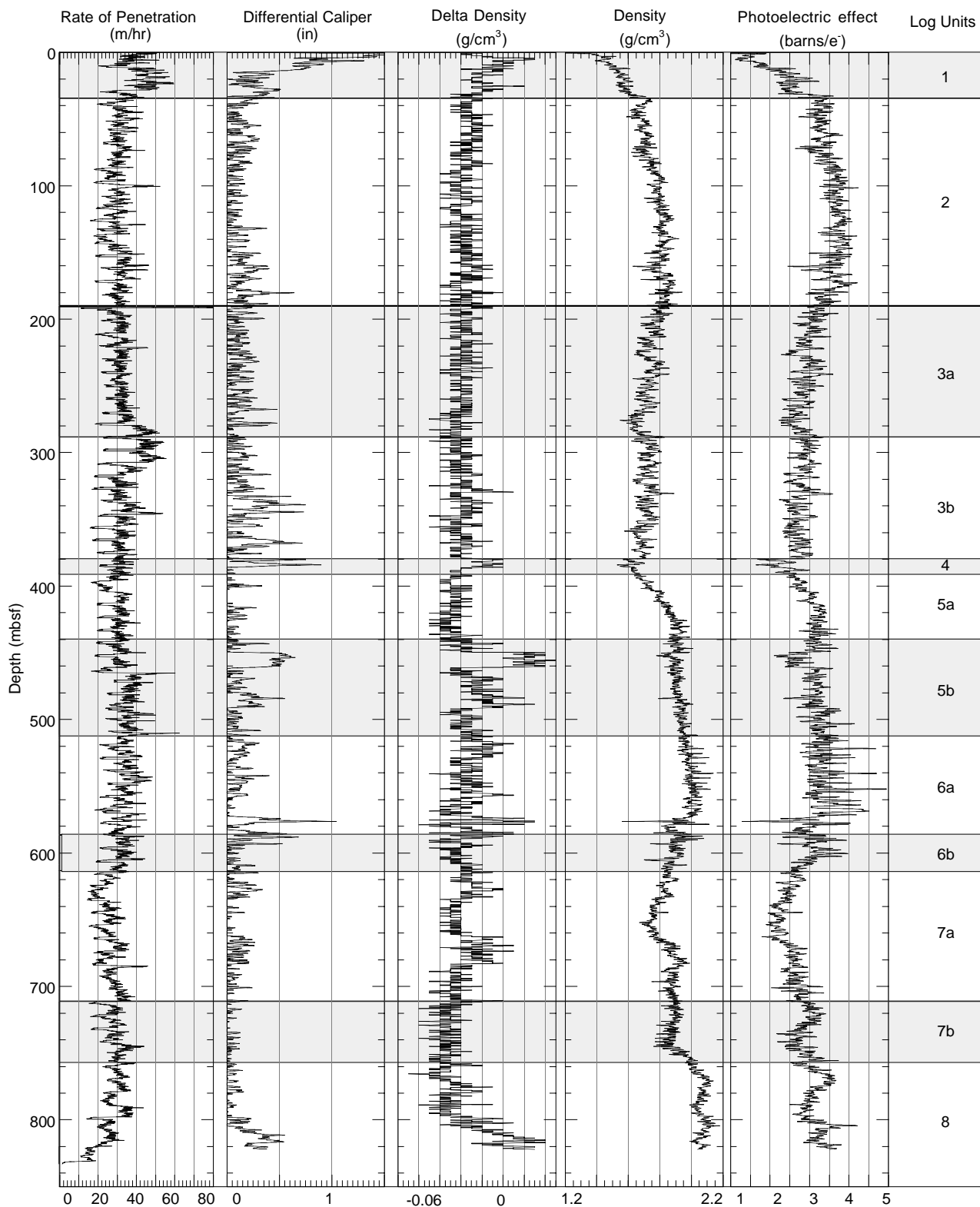


Figure 6. Site 1046 LWD data and log units. Post-cruise processed log data are available on CD-ROM (back pocket, this volume).

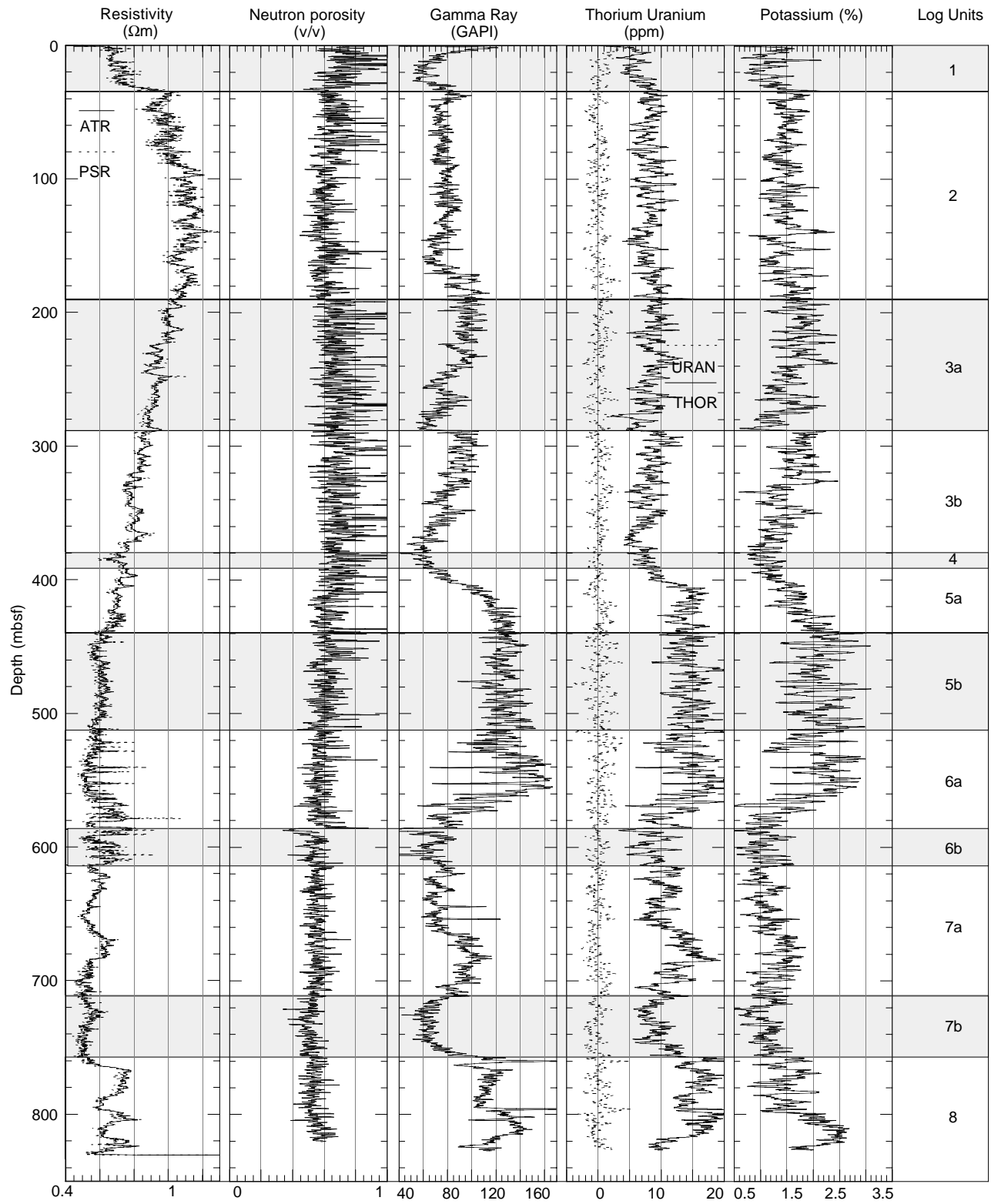


Figure 6 (continued).

**Table 1. Mean values and standard deviations of the log properties according to each cluster for Hole 1046A.**

	ATR ( $\Omega\text{m}$ )		GR (GAPI)		THOR (ppm)		POTA (%)		PEF		ROMT ( $\text{g}/\text{cm}^3$ )		TNPH (v/v)	
	Mean	SD	Mean	SD	Mean	SD	Mean	SD	Mean	SD	Mean	SD	Mean	SD
All	0.77	0.20	92.22	24.82	10.67	3.57	1.55	0.45	3.04	0.45	1.83	0.12	0.60	0.06
Cluster 1	0.88	0.10	81.92	13.48	8.39	1.90	1.54	0.33	2.86	0.28	1.71	0.06	0.65	0.06
Cluster 2	1.08	0.07	78.64	8.49	8.04	1.42	1.45	0.23	3.60	0.23	1.79	0.05	0.60	0.04
Cluster 3	0.57	0.05	80.67	15.07	11.12	2.60	1.20	0.25	2.55	0.29	1.85	0.08	0.55	0.03
Cluster 4	0.63	0.07	124.62	15.78	14.94	2.36	1.96	0.45	3.18	0.27	1.97	0.08	0.58	0.05
Cluster 5	0.63	0.08	66.59	14.67	8.15	1.96	0.99	0.28	3.33	0.46	1.93	0.08	0.51	0.04

Notes: SD = standard deviation; ATR = deep resistivity; GR = gamma ray; THOR = thorium; POTA = potassium; PEF = photoelectric effect; ROMT = density (rotationally processed); TNPH = thermal neutron porosity.

Fig. 11A) also occur at Site 1044 and are believed to be dominated by primary depositional processes unrelated to deformational features in the toe of the prism.

### Photoelectric Effect

As at Sites 1044 and 1045, the photoelectric effect log for Site 1046 closely mimics the pattern in the density log (Fig. 12). However, as a result of the different physical principles of the measurement, the photoelectric effect log seems to be more sensitive to the occurrence of high-porosity, low-density zones. This is apparent at several of the thrust faults and also just above the top of the décollement zone.

### Comparison of Core and Log Density Data

At Site 1046 we redrilled section partially recovered at Site 949 (Shipboard Scientific Party, 1995b); therefore, it was possible to compare the density log with the core wet bulk density data (Fig. 13). The superimposed log and core data agree remarkably well. However, all wet bulk density measurements of Core 156-949B-7X (302–311 mbsf) are clearly offset to higher density values by about 0.1–0.2  $\text{g}/\text{cm}^3$  (Fig. 13). The reason for this deviation is unclear, but the higher carbonate content (Fig. 2) may be responsible for this mismatch.

### Resistivity Logs

The deep and shallow resistivity logs are identical in character, although the former has a lower resolution, giving it a smoothed appearance. The overall resistivity trend is an increase from the seafloor to about 1.1  $\Omega\text{m}$  at 100 mbsf (Fig. 11B). The trend remains constant at 1.1  $\Omega\text{m}$  to 140 mbsf and then gradually decreases to a low of 0.5  $\Omega\text{m}$  at 765 mbsf. Resistivity increases in the interval below 767 mbsf to 0.75  $\Omega\text{m}$  at 823 mbsf. The resistivity curves are offset slightly in some intervals, most notably at 265–288, 345–423, and 767–823 mbsf. The deep resistivity is higher than the shallow resistivity by as much as 0.05  $\Omega\text{m}$  in these offsets.

The variability of the resistivity changes within the log. The interval 0–190 mbsf (log Units 1 and 2) has a high variability, with a standard deviation of 0.069  $\Omega\text{m}$  in the deep resistivity. The interval that contains turbidites (~512–615 mbsf, log Unit 6), has large spikes in the resistivity curves and a high standard deviation (0.077  $\Omega\text{m}$  in the deep resistivity). Log Subunit 7a has low variability, with a standard deviation of 0.055  $\Omega\text{m}$ .

The décollement zone (380–390 mbsf, log Unit 4) is not well defined in the resistivity logs. There is a slight negative shift from the overall trend of 0.05  $\Omega\text{m}$  at the décollement zone, with two low spikes below 0.6  $\Omega\text{m}$ .

### Comparison of the Proto-Décollement Zone at Site 1044 With the Décollement Zone at Site 1046

To examine the change in physical properties as sediments are loaded by accretion, density and resistivity from the décollement

zone at Site 1046 were compared with those at Site 1044 (Fig. 14A, B). We used the same scale that was used for Figure 14B to facilitate a comparison among the three sites. In contrast to Site 1045, correlation of Site 1046 with the reference site is uncertain. The depth shift was made by aligning the proposed top of the Site 1046 décollement zone (at 380 mbsf) to the top of the Site 1044 proto-décollement zone. In general, the density values measured at the décollement zone at Site 1046 exceed those at the décollement zone at Site 1044 by more than 0.2  $\text{g}/\text{cm}^3$ . Resistivities from the décollement zone at Site 1046 exceed those of the reference site, whereas, in general, Site 1046 resistivities are lower than those at the reference site.

### Comparison of Underthrust Section at Sites 1046 and 1044

The density, resistivity, and photoelectric effect logs directly below the décollement zone (427 mbsf to total depth) are similar to those from 70 m below the proto-décollement zone at Site 1044 (300 mbsf to total depth). At both sites there are rapid, large variations attributed to turbidites, overlying broad lows and highs attributed to lithologic variations (see “Logs and Lithology” section, this chapter). Relative to Site 1044, the 70-m shift observed at Site 1046 may reflect lateral facies change of the uppermost part of the underthrust section between the two sites.

### Summary

1. The density log agrees with all available core densities, except those from the carbonate-rich zone at 300–322 mbsf (Core 156-949B-7X).
2. Density, resistivity, and photoelectric effect show discontinuities at 42, 285, and 382 mbsf that correlate with faults identified in core and seismic sections.
3. Within the décollement zone, density has a low at the top and then increases sharply with depth from 380 to 432 mbsf; resistivity falls within the same interval.
4. Density, resistivity, and photoelectric effect logs from the underthrust sediments below 427 mbsf are closely correlated with those from 70 m below the proto-décollement zone at reference Site 1044.

### LOGS AND INDICATORS OF FLUID FLOW

At Site 1046, LWD was used to collect continuous data where previous drilling (Site 949) obtained poor core recovery. CORK data from this location indicate overpressures of 1 MPa ( $\lambda^* = 0.3$ ) and a high thermal gradient of 82°C/km from 200 to 500 mbsf across the décollement zone (Becker et al., 1997). The thermal gradient is linear and shows no evidence of any thermal transients (Shipboard Scientific Party, 1995b). Despite poor recovery, core data from Site 949 provide geochemical evidence for fluid flow along fault zones. Figure 15 shows the geochemical data from Site 949, along with the density, gamma-ray, and resistivity LWD logs from Site 1046. In this

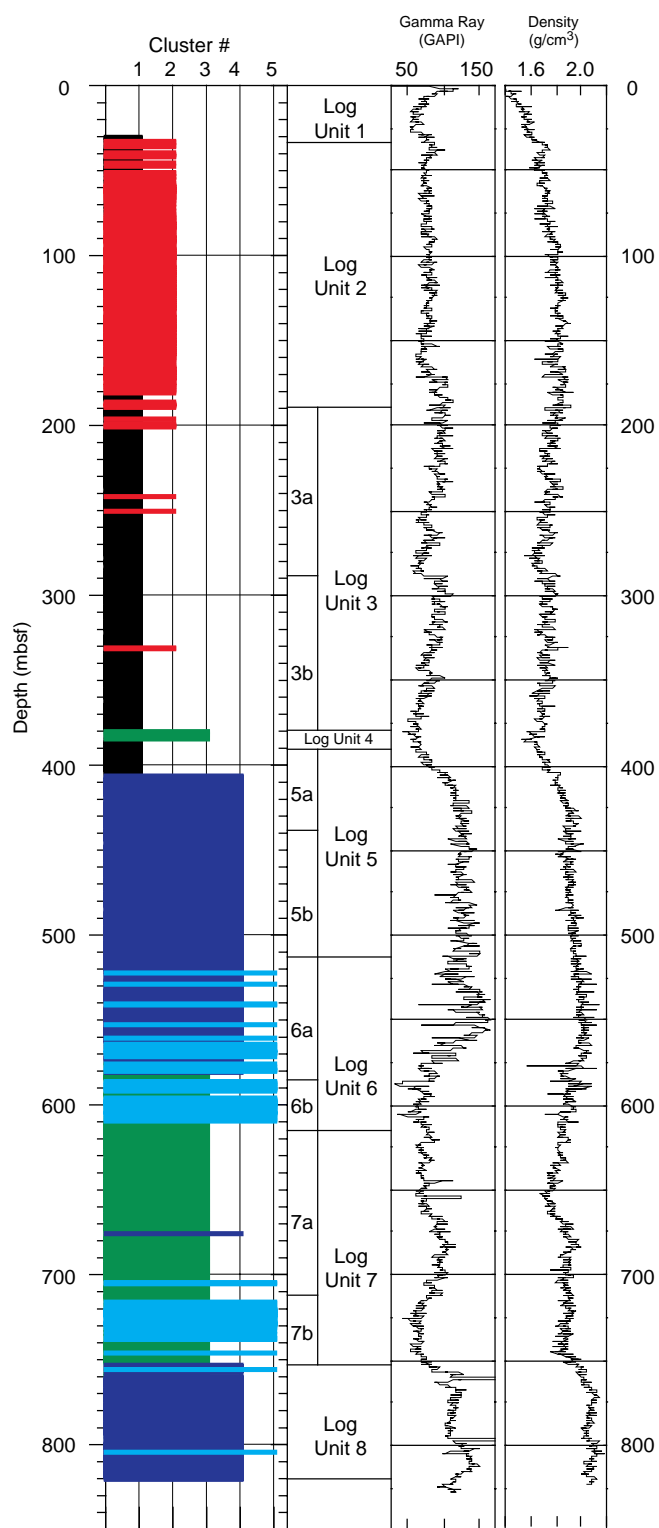


Figure 7. Definition of log units for Site 1046. Five clusters were derived from three factor logs that account for 90% of the total variance observed in the data. Boundaries between first-order log units correspond to changes in log character that are related primarily to lithology and that are clearly visible on logs (e.g., gamma ray, density, photoelectric effect, and resistivity). Second-order units represent subtle changes in log character that are observed in only a few curves and that may not be related to lithology.

section, we discuss the LWD results for fluid-flow paths proposed on the basis of Site 949 core data.

### Thrust Faults

In Hole 949B, the uppermost interstitial-water sample, which was collected at 245.5 mbsf, indicates below-seawater chloride values. Elevated methane values were also obtained just above this depth at 244.1 mbsf. The LWD data from Hole 1046A show reduced density at 225 mbsf and several resistivity lows from 220 to 245 mbsf, suggesting a thrust zone at this location (see “Logs and Structure” section, this chapter).

Low chloride values were also measured at 288.6 mbsf, and elevated methane was measured at nearby depths. These geochemical observations correlate reasonably well with the LWD data, which indicate reduced density and gamma ray from 280 to 287.9 mbsf (the boundary between log Subunits 3a and 3b). Interpretation of the seismic profile also suggests the presence of a thrust fault at 286 mbsf (see “Logs and Structure” section, this chapter). The chloride data suggest that the maximum age of the thrust is ~36 ka (Shipboard Scientific Party, 1995b). Moreover, the linear thermal profile suggests that sufficient time has passed for diffusion to smooth any disruption in the thermal profile.

Chloride values are below that of seawater from 350 to 380 mbsf, whereas methane values are highly variable. A particularly low chloride value of 530 mM was measured at 358.6 mbsf. This correlates with core structural observations, which indicate shear fabrics at 355 mbsf. Similarly, the LWD data show resistivity and gamma-ray highs at ~350 mbsf, and the differential caliper data suggest widening of the borehole at this depth interval.

### Décollement Zone

Seismic data and structural observations from Hole 949B indicate a broad zone of deformation between 370 and 427 mbsf, but poor core recovery precludes a more precise localization of the décollement zone. As noted previously, chloride values within Holes 949B and 949C are generally low beneath 350 mbsf, and this trend persists to ~432 mbsf. The highest measured methane values from Site 949 occur just below 400 mbsf. The LWD data show density, gamma-ray, and photoelectric effect lows from 380 to 390 mbsf. Over this interval, there was no core recovery, and consequently there are no geochemical data. The LWD density, gamma-ray, and photoelectric effect values then rise sharply from 390 to 420 mbsf, where the increase then becomes more gradual. A pronounced spike in dissolved silica concentration at 402 mbsf is probably a good indicator of the center of the radiolarian-rich layer that correlates with the décollement zone.

The density logs from the décollement zone at Sites 1044 and 1046 are shown in Figure 14 (see “Logs and Physical Properties” section, this chapter). Only a small remnant of the underconsolidation inferred in Hole 1044A is observed near the top of the décollement zone in Hole 1046A. Moreover, the extent of consolidation in the décollement zone in Hole 1046A is significantly greater than that in Hole 1045A, although Site 1046 would have been incorporated into the complex ~50 k.y. later than Site 1045. This indicates that there is a significant difference between the hydrologic regimes of the décollement zone at Sites 1045 and 1046.

### Underthrust Sediments

Two chloride measurements and one methane measurement from below 450 mbsf have background concentrations. Thus, there is no downward flow from the décollement zone to the underthrust at this location. The next significant flow path indicated by the LWD data and previous drilling results lies along the turbidite sequences identi-

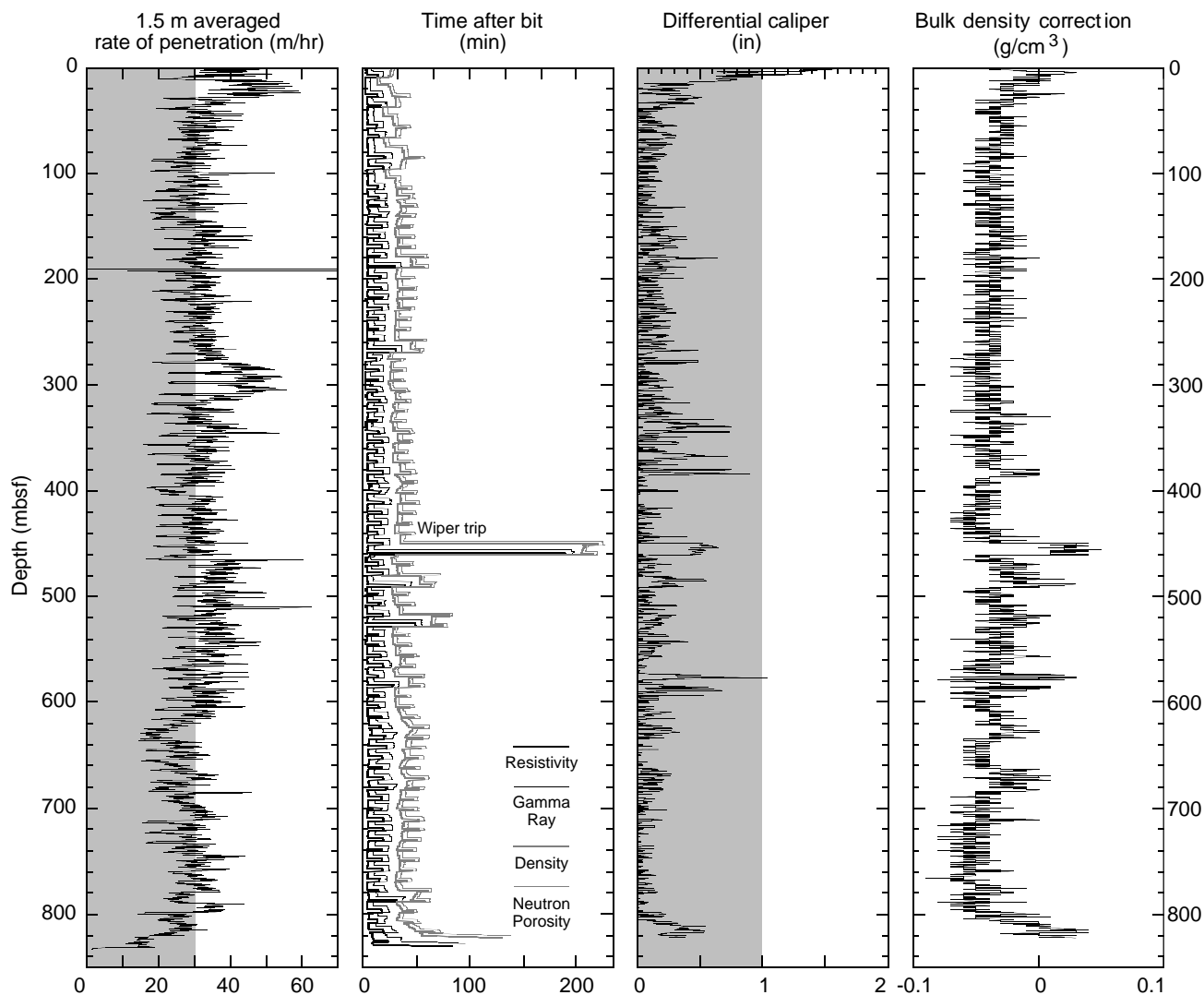


Figure 8. Summary of the quality-control logs. The shaded area in the ROP shows the reliable zone for NGT measurements according to industry experience. The shaded area in the differential caliper indicates good borehole conditions.

fied in log Subunits 6a and 6b (512–613 mbsf). The caliper log exceeds 1 in at 575 mbsf, indicating a possible increase in formation pressure, although this could also be because of a change to sandy lithology. The LWD data show that the turbidites present at Site 1044 are also present at this site. The high thermal gradient measured at Site 949 (Fig. 1) is consistent with the migration of warm fluids, but the linearity of the temperature profile suggests that the flow of warm fluids has not occurred in the section above 500 mbsf. Thus, at this site, the turbidite sequences, rather than the décollement zone, represent the most likely conduit for the flow of warm fluids.

### Summary

1. Pore-water chemical anomalies at 288.6 mbsf appear to correlate with a zone of low-density and gamma-ray values observed in the LWD data and a thrust fault observed on the seismic profile. Thus, there is strong evidence that the change in character of the log data corresponds to a fluid-flow conduit along the fault.
2. In the décollement zone, broad chemical anomalies, a linear temperature profile, and high densities observed on the LWD logs all argue for no recent significant fluid flow from depth.

3. The turbidites in the underthrust section, rather than the décollement zone, may currently be a more active conduit for warm fluid migration.

## LOGS AND SEISMIC DATA

### Synthetic Seismogram

The synthetic seismogram for Site 1046 was constructed using an assumed velocity profile, as described in the “Explanatory Notes” chapter (this volume). At Site 1046 the velocity profile consists of a linear gradient from 1.5 km/s at the seafloor to 2.1 km/s at the bottom of the hole. This is the same gradient that was used at Sites 1044 and 1045.

The synthetic seismogram shows a reasonably good match to the décollement reflection observed in the 3-D seismic data at this site (Fig. 16). Several reflections in the upper 300 mbsf of the synthetic seismogram correlate with dipping reflections in the seismic data, although the amplitudes in the seismic data are much lower than those in the synthetic seismogram. A strong negative polarity reflection in the synthetic seismogram is created by the density drop at 275 mbsf and correlates with a strong negative polarity reflection that has a

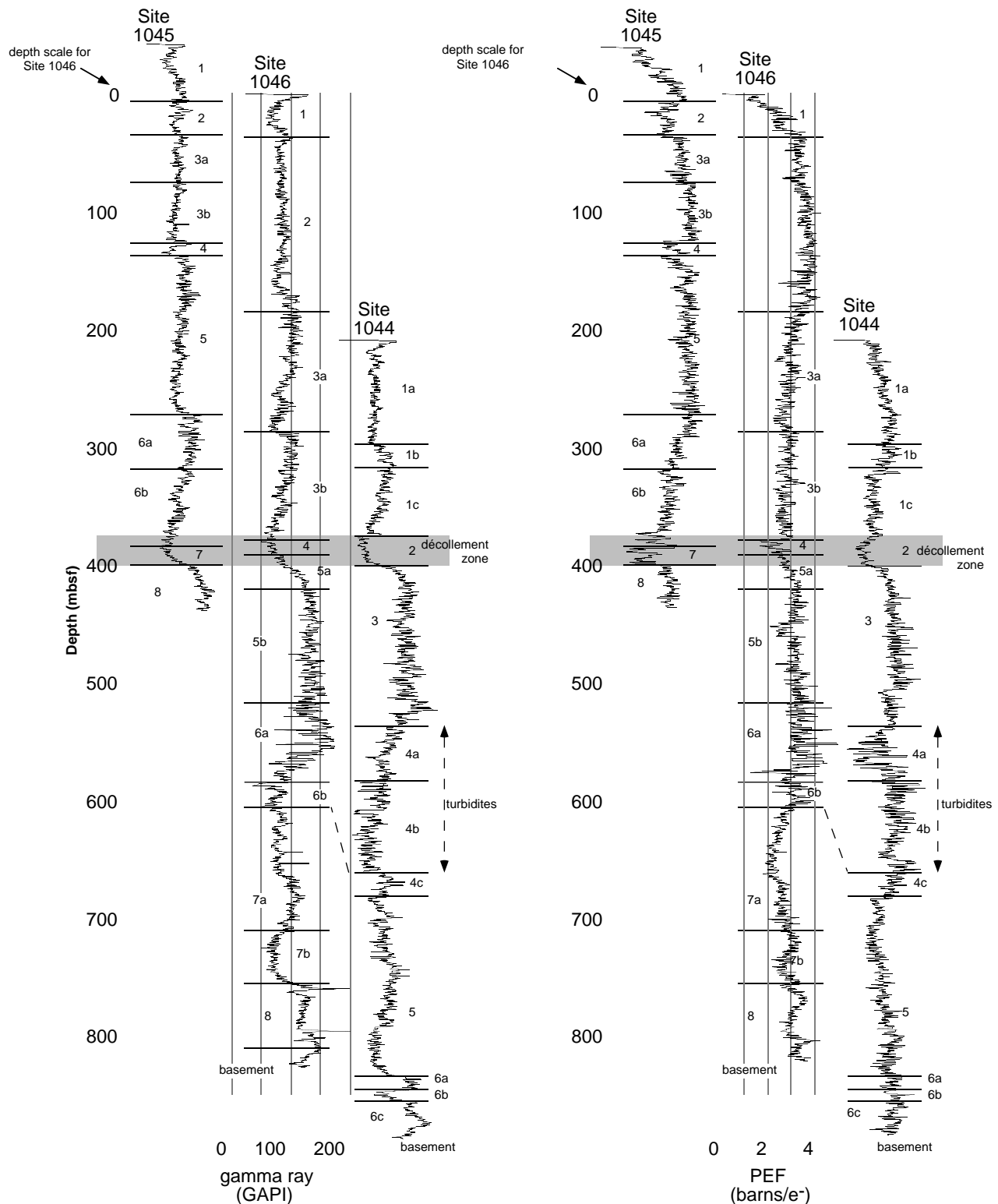


Figure 9. LWD gamma-ray and photoelectric effect logs from Sites 1045 and 1044 compared with the section logged at Site 1046. The Site 1045 gamma-ray and photoelectric effect logs are shifted up by 50 m, and the same logs from Site 1044 are shifted down by ~180 m to align the décollement zone level at all three sites. Both Sites 1044 and 1046 were drilled to basement (but not into basement). The upper section at Sites 1046 and Site 1045 are similar, as are the logs through the underthrust section. Dashed lines show possible tie-points between the turbidite units at Sites 1044 and 1046. See text for further discussion. The logs are the same scale, but the depth scale refers only to the Site 1046 logs (see "Site 1044" and "Site 1045" chapters [this volume] for the exact depth of the unit boundaries at these sites).

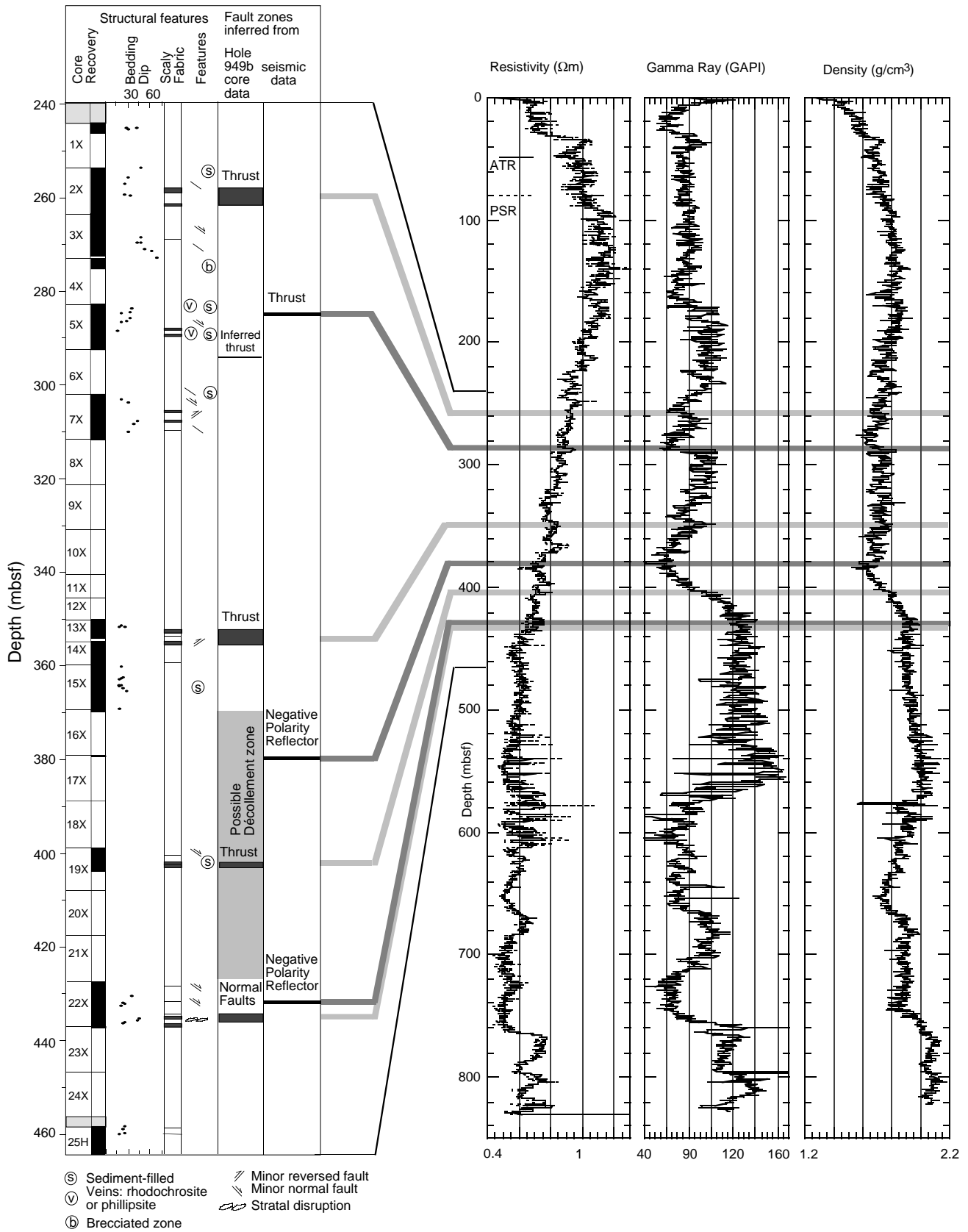


Figure 10. Structural synthesis of Hole 949B, and the relationship among faults identified in cores (light lines), seismic reflection data (dark lines), and Hole 1046A LWD logs. The two faults (dashed lines) at 162 and 225 mbsf are inferred from the LWD log data.

**Table 2. Bulk density profile division with mean values and standard deviations.**

Depth (mbsf)	Mean density (g/cm <sup>3</sup> )	Standard deviation (g/cm <sup>3</sup> )	Characteristics	Comments
0-42	1.56	0.11	Steady increase	Normal consolidation
42-162	1.77	0.06	Gradual increase	Normal consolidation
162-225	1.77	0.06	Slight decrease	Anomalous porosity-depth trend
225-285	1.71	0.06	Slight decrease	Repeat section
285-350	1.73	0.05	No density change with depth	Directly above décollement zone
350-380	1.68	0.06	Steep increase in density	
380-432	1.77	0.16	Gradual increase in density	Correlates with Site 1044
432-570	1.95	0.15	Gradual decrease in density	Correlates with Site 1044
570-650	1.86	0.16	Decline in density	Correlates with Site 1044
650-680	1.81	0.08	Steep increase in density	Correlates with Site 1044
680-745	1.88	0.05	No change with depth	Correlates with Site 1044
745-770	1.99	0.03	Slight increase	Correlates with Site 1044
770-TD	2.07	0.15	Unclear development with depth	

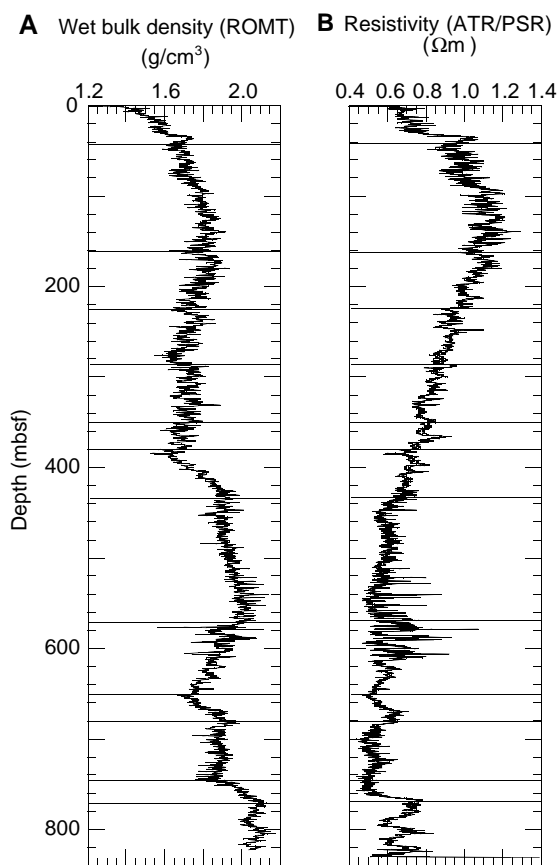


Figure 11. (A) Bulk density and (B) resistivity vs. depth in Hole 1046A. Lines separate intervals discussed in the text.

thrust at its base in the seismic data. The negative polarity reflection at 5300 mbsl (575 mbsf) in the synthetic trace correlates well with a horizontal reflection at 5320 mbsl (595 mbsf) at common midpoints 1222–1225, but the amplitude of this reflection is very low near the drill site.

The décollement zone is not well imaged either in the seismic data or the synthetic seismogram at Site 1046. The structural décollement zone is probably between the two negative polarity reflections at 5405 and 5460 mbsl (380–435 mbsf) in the seismic data, neither of which appears in the synthetic trace. The low-amplitude, negative polarity reflection at 5440 mbsl (415 mbsf) in the synthetic seismogram is generated by a corresponding drop in density in the log data. This drop in density is at the base of a zone of gradually increasing density that characterizes the lower limit of the décollement zone.

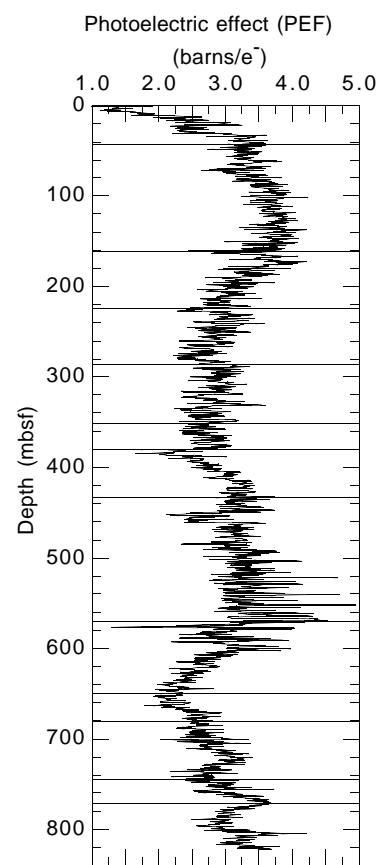


Figure 12. Photoelectric effect vs. depth in Hole 1046A. Lines separate intervals discussed in the text.

Several low-amplitude reflections below the décollement zone correlate with reflections in the synthetic trace, but the major feature in the synthetic trace, a high-amplitude negative reflection at 5600 mbsl (575 mbsf), does not correlate with any nearby reflections in the seismic data. This reflection, generated by the decrease in density at 580 mbsf, correlates with a strong reflection from the inferred turbidite interval at this depth at common midpoints 1212–1216.

#### REFERENCES

- Becker, K., Fisher, A.T., and Davis, E.E., 1997. The CORK experiment in Hole 949C: long-term observations of pressure and temperature in the Barbados accretionary prism. In Shipley, T.H., Ogawa, Y., Blum, P., and Bahr, J.M. (Eds.), *Proc. ODP, Sci. Results*, 156: College Station, TX (Ocean Drilling Program), 247–254.

Bekins, B.A., McCaffrey, A.M., and Driess, S.J., 1995. Episodic and constant flow models for the origin of low-chloride waters in a modern accretionary complex. *Water Resour. Res.*, 31:3205–3215.

Screaton, E.J., Fisher, A.J., Carson, B., and Becker, K., 1997. Barbados Ridge hydrogeologic tests: Implications for fluid migration along an active décollement. *Geology*, 25:239–242.

Screaton, E.J., Wuthrich, D.R., and Dreiss, S.J., 1990. Permeabilities, fluid pressures, and flow rates in the Barbados Ridge Complex. *J. Geophys. Res.*, 95:8997–9007.

Shipboard Scientific Party, 1995a. Explanatory notes. In Shipley, T.H., Ogawa, Y., Blum, P., et al., *Proc. ODP, Init. Repts.*, 156: College Station, TX (Ocean Drilling Program), 39–68.

\_\_\_\_\_, 1995b. Site 949. In Shipley, T.H., Ogawa, Y., Blum, P., et al., *Proc. ODP, Init. Repts.*, 156: College Station, TX (Ocean Drilling Program), 193–257.

Tribble, J.S., 1990. Clay diagenesis in the Barbados accretionary complex: potential impact on hydrology and subduction dynamics. In Moore, J.C., Mascle, A., et al., *Proc. ODP, Sci. Results*, 110: College Station, TX (Ocean Drilling Program), 97–110.

Underwood, M.B., and Deng, D., 1997. Clay mineralogy and clay geochemistry in the vicinity of the décollement zone, ODP Leg 156, northern Barbados Ridge. In Shipley, T.H., Ogawa, Y., Blum, P., and Bahr, J.M., et al., *Proc. ODP, Sci. Results*, 156: College Station, TX (Ocean Drilling Program), 3–32.

Ms 171AIR-105

**NOTE: For all sites drilled, shore-based log processing data are available on CD-ROM. See Table of Contents for material contained on CD-ROM.**

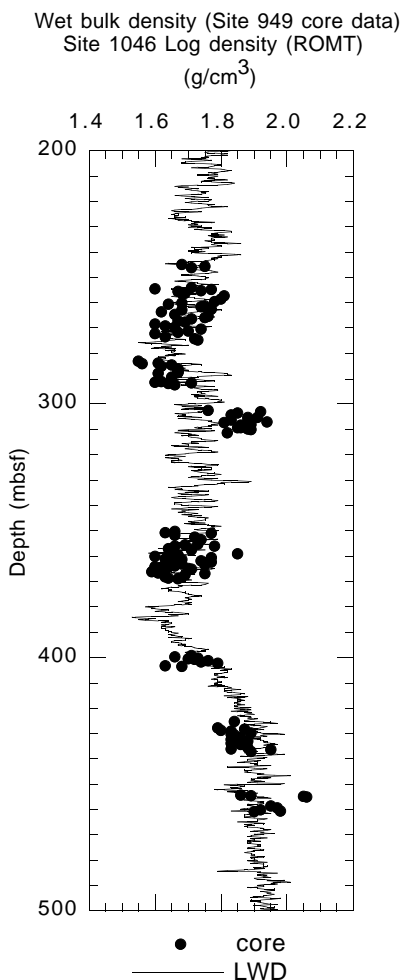


Figure 13. Bulk density vs. depth in Hole 1046A compared with core wet bulk density from Site 949.

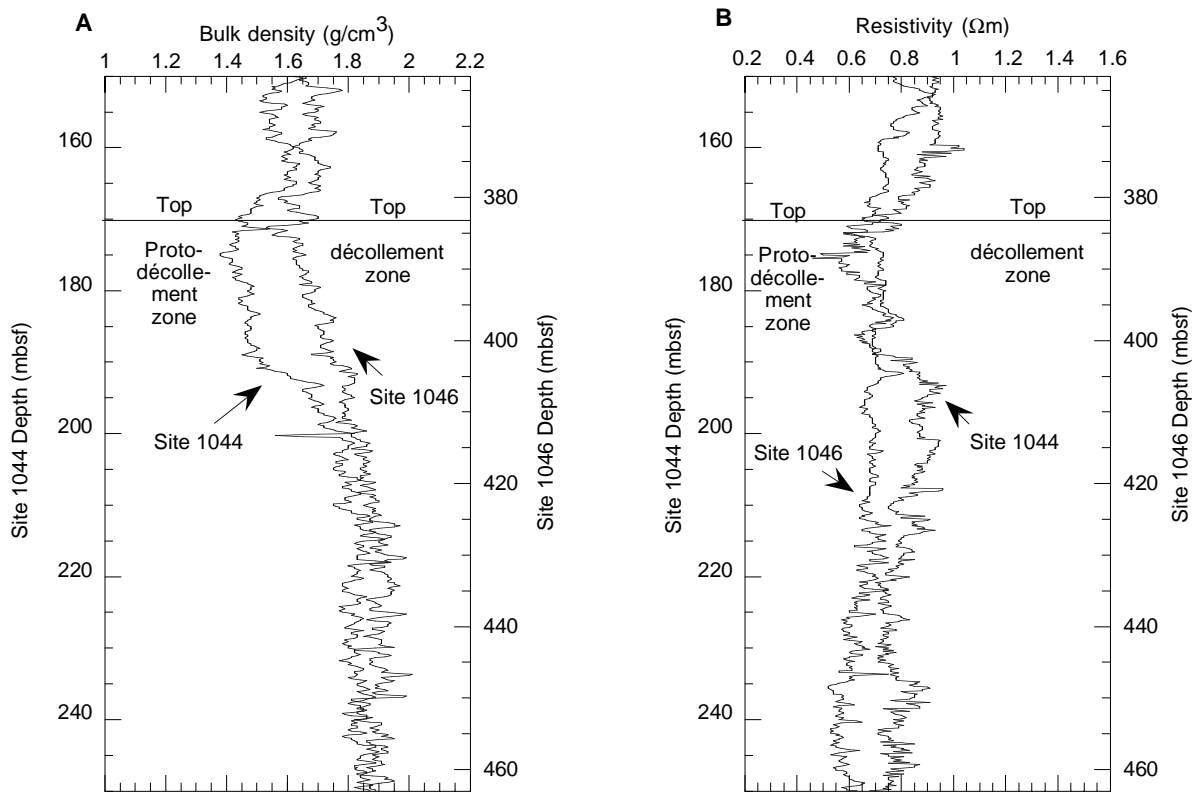


Figure 14. Comparison of (A) wet bulk density and (B) resistivity across the proto-décollement zone at Site 1044 and the décollement zone at Site 1046.

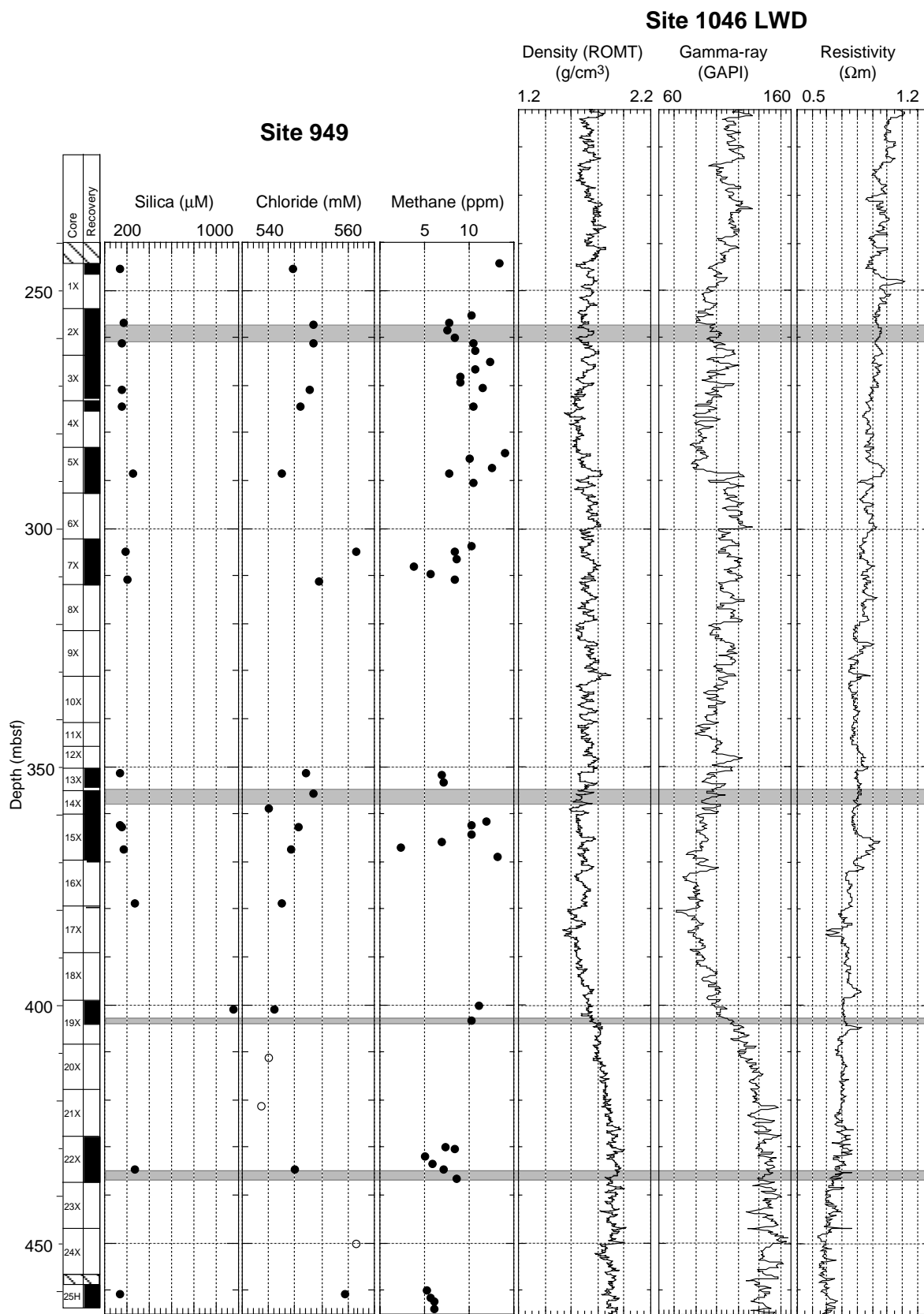


Figure 15. Comparison of LWD data from Hole 1046A with geochemical results from Site 949. The shaded areas indicate faults interpreted from core data.

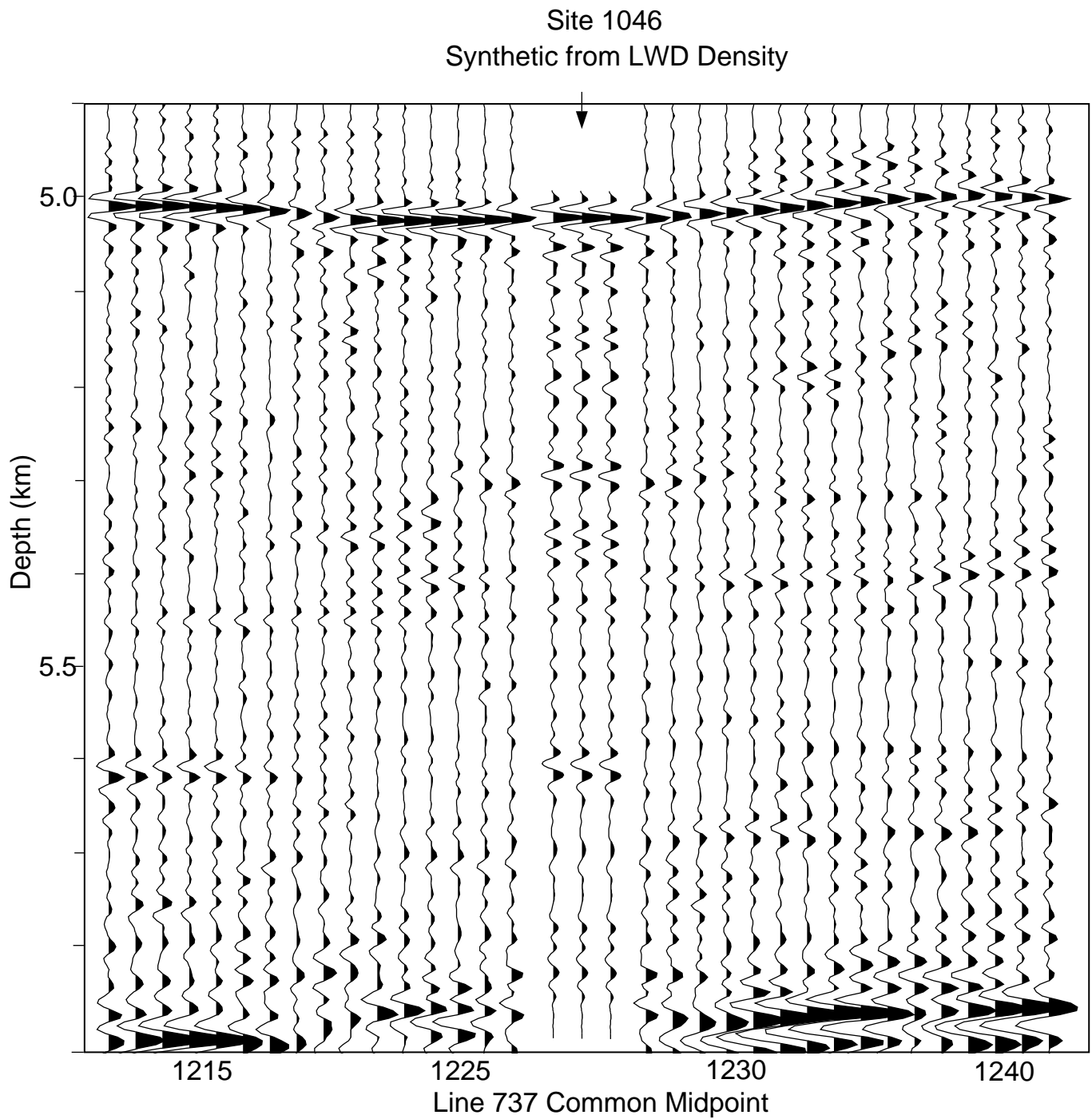


Figure 16. Three identical synthetic traces are shown at the location of Site 1046 on Line 737. See "Explanatory Notes" chapter (this volume) for description of the synthetic seismogram construction. Trace spacing is 15 m; vertical exaggeration is 2x.